WARSAW UNIVERSITY OF TECHNOLOGY Index 351733
FACULTY OF CIVIL ENGINEERING
COMMITTEE FOR CIVIL AND WATER ENGINEERING
POLISH ACADEMY OF SCIENCES ISSN 1230-2945
DOI: 10.24425/ace.2023.144169
ARCHIVES OF CIVIL ENGINEERING
Vol. LXIX ISSUE 1 2023

pp. 213 –229

Research paper

Experimental study on biaxial dynamical compressive test and PFC^{2D} numerical simulation of artificial rock sample with single joint

Xiong Liangxiao[1], Haijun Chen[2], Xinghong Gao[3], Zhongyuan Xu[4], Deye Hu[5]

Abstract: Dynamic biaxial compression tests and Particle Flow Code numerical simulations of the cement mortar specimens with a single joint were carried out to study the mechanical properties and crack evolution of artificial rock samples with a single joint. The effects of lateral stress σ_2, loading rate V, the dip angle β (between the vertical loading direction and the joint) on the biaxial compressive strength σ_b, and the evolution law of crack were investigated. Test results showed that; (1) when both the dip angle β and the loading rate V remained unchanged, the biaxial compressive strength σ_b increased with the increase in the lateral stress σ_2, while σ_2 had no obvious effect on the crack evolution law; (2) when both the dip angle β and the lateral stress σ_2 were kept unchanged, the loading rate V had an insignificant effect on the biaxial compressive strength σ_b and the crack evolution law; (3) when both the lateral stress σ_2 and the loading rate V were constant, the biaxial compressive strength σ_b decreased first and then increased with the increase in the dip angle β; however, the dip angle β did not significantly affect the crack evolution law. The conclusions obtained in this paper are presented for the first time.

Keywords: artificial rock specimen, biaxial dynamic compression, compressive strength, crack evolution law

[1]Associate Prof., PhD., Eng., School of Civil Engineering and Architecture, East China Jiaotong University, Nanchang 330013, China, e-mail: xionglx1982@126.com, ORCID: 0000-0002-6366-5187
[2]Prof., PhD., Eng., Geotechnical Engineering Department, Nanjing Hydraulic Research Institute, Nanjing, 210029, China, e-mail: hjchen@nhri.cn, ORCID: 0000-0003-0094-9649
[3]Eng., China Construction Third Bureau First Engineering Co., Ltd., Wuhan 430040, China, e-mail: 767590414@qq.com, ORCID: 0000-0002-9906-1086
[4]PhD, Faculty of Geosciences and Environmental Engineering, Southwest Jiaotong University, Chengdu 611756, China, e-mail: zyxu@swjtu.edu.cn, ORCID: 0000-0003-4303-1870
[5]BEng., School of Civil Engineering and Architecture, East China Jiaotong University, Nanchang 330013, China, e-mail: 2573713909@qq.com, ORCID: 0000-0001-8132-0812

1. Introduction

When the tunnel is excavated and not supported yet, the surrounding rock of the tunnel is in a biaxial compression state. The study of the mechanical properties of the rock under biaxial compression provides significant guidance for tunnel support design. At the same time, the surrounding rock of the tunnel usually contains joints. Therefore, studying the mechanical properties and the crack evolution of jointed rock mass under biaxial compression is necessary.

At present, many researchers have performed uniaxial compression tests on rock specimens with joints. Kulatilake *et al*. [1] performed laboratory experiments to study the behavior of jointed blocks of model material under uniaxial loading, and three modes of failure were identified in the laboratory experiments. Lee *et al*. [2] carried out uniaxial compression tests on three different specimen types containing single and double flaws. They found that the shielding effect of the horizontal flaw played an important role in the stresses of specimens. Chen *et al*. [3] conducted a series of uniaxial compression tests on gypsum specimens with regularly arranged multiple pre-existing parallel joints, and seven types of crack initiation were identified in this test. Cao *et al*. [4] investigated the uniaxial compressive strength and failure patterns of ubiquitous-joint rock-like specimens by combining similar material testing and numerical simulations. They found that under uniaxial compression, the failure patterns of ubiquitous-joint specimens can be classified into four categories. Through uniaxial compression experiments, Yang *et al*. [5] found that the peak strength and elastic modulus of sandstone specimens containing two noncoplanar fissures were lower than those of intact specimens. Zhao *et al*. [6] carried out a series of uniaxial compression tests on rock-like specimens containing two flaws, and four different types of cracks and seven crack coalescence patterns were observed in the experiments. Zhang *et al*. [7] conducted uniaxial compressive tests on reinforced analog specimens with cross flaws and with a single flaw. They found that the reinforced rock mass with cross flaws exhibited higher uniaxial compressive strength than that of reinforced rock mass with a single flaw. Huang *et al*. [8] studied the mechanical behaviors of the brittle rock-like specimens with multi-nonpersistent joints under uniaxial compression. The results showed that the inclined joint angle significantly influenced uniaxial compressive strength and Young's modulus.

In addition, several researchers conducted triaxial compression tests on rock specimens with joints. Yang *et al*. [9] carried out conventional triaxial compression tests on sandstone specimens containing two pre-existing three-dimensional flaws. They found that the strength properties of pre-flawed sandstone specimens were closely related to the flaw angle and confining pressure. Xiang *et al*. [10] carried out a series of triaxial compression tests on rock-like specimens with hidden smooth joints under triaxial compression. They found that the presence of hidden joints led to a large strength and deformation modulus reduction of the specimen. Yao *et al*. [11] conducted uniaxial and triaxial compressive experiments on intact and single- and double-flawed granite specimens and found that under constant confining pressure, the peak stress of flawed specimens decreased with the increase in the prefabricated flaw number.

Furthermore, few researchers conducted biaxial compression tests on rock specimens with joints. Prudencio and Van Sint Jan [12] performed biaxial tests on physical models of rock with nonpersistent joints. Therefore, the achievements of biaxial compression tests on rock specimens with fractures are still seldom.

Many researchers used Particle Flow Code (PFC) to numerically simulate rock samples with joints under uniaxial compression and triaxial compression. Fan *et al*. [13] studied crack initiation stress and strain of jointed rock containing multi-cracks under uniaxial compressive loading by applying numerical analysis using PFC^{3D}. Yang *et al*. [14] investigated the failure behavior of brittle sandstone specimens containing three fissures under uniaxial compression by discrete element modeling. Cao *et al*. [15] carried out numerical simulations using PFC^{2D} to model the crack coalescence and failure model of multi-fissure specimens under uniaxial loading. Yang *et al*. [16] conducted a numerical simulation of rock blocks with nonpersistent open joints under uniaxial compression using the particle flow modeling method.

More uniaxial and triaxial compression tests and numerical simulations have been carried out on rock samples with prefabricated joints, but few biaxial compression tests and numerical simulations have been carried out. The main difficulty in the biaxial compression test is determining the test scheme. We conducted biaxial dynamic compression tests and PFC numerical simulations on cement mortar specimens with prefabricated cracks to investigate the mechanical properties and crack evolution law of rock with cracks under biaxial compression. It was aimed to study the influence of lateral stress σ_2, loading rate V, and inclined angle β of prefabricated crack on the biaxial compressive strength and crack evolution law of the specimen. The research results of this paper will supplement and enrich the research results of the rock biaxial compression test and numerical simulation. In previous studies, authors mainly carried out uniaxial compression tests and numerical simulations for rock-like rocks with cracks. In this paper, we mainly designed biaxial compression tests and performed numerical simulations for rock-like rocks with cracks. This is the same point and difference between this paper and our previous research results.

2. Test principle

2.1. Sample preparation

The size of the specimen was 100 mm × 100 mm × 100 mm. The prefabricated crack was formed by a plastic piece with a thickness of 1 mm, and the length of the plastic piece was 120 mm. The specimen was made of cement mortar with a water/cement ratio of 0.65. We used Portland cement #325 and quartz sand in the tests.

After 2 hours of the initial setting of the cement mortar, the plastic piece was inserted according to the location of the crack in Figure 1; after another 12 hours, the plastic piece was pulled out, and a prefabricated joint formed in the specimen.

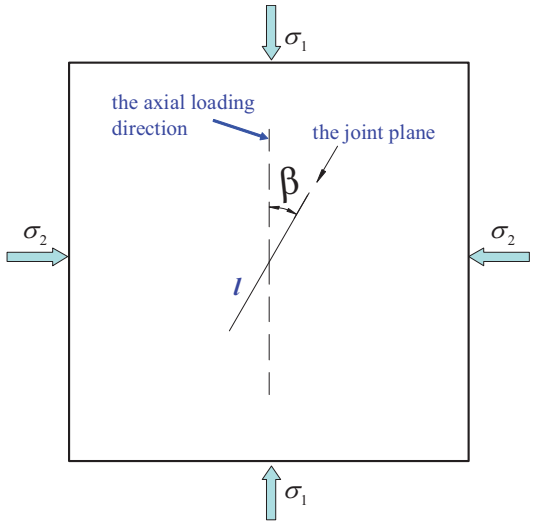

Fig. 1. The relationship between the loading direction and joint plane

In Figure 1 and the later part of this study, the length of the crack is defined as l and fixed as 4 mm; the angle between the joint and vertical loading direction is defined as β, and β ranged from 0 to 90°; σ_1 is the vertical stress, and σ_2 is the lateral stress.

2.2. Test equipment

After 28 days of standard curing, the test specimens were placed for 7 days out of the furnace, and then biaxial compression tests were applied to these specimens. The biaxial compression test machine is shown in Figure 2.

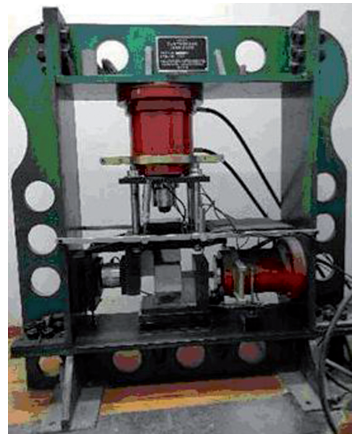

Fig. 2. The biaxial compression test machine

2.3. Test groups

During the biaxial compression test, the axial loading rate was the same as the lateral loading rate, and both of them are defined as V. The test was mainly grouped according to the inclined angle β of the joint, the lateral stress σ_2, and the loading rate V. The test groups are shown in Table 1.

Table 1. Biaxial compression test groups

Study	β (°)	σ_2 (MPa)	V (KN/s)
1	0, 30, 45, 60, 90	0, 2, 4, 6, 8	2
2	0, 30, 45, 60, 90	0, 2, 4, 6, 8	4
3	0, 30, 45, 60, 90	0, 2, 4, 6, 8	6
4	0, 30, 45, 60, 90	0, 2, 4, 6, 8	8
5	0, 30, 45, 60, 90	0, 2, 4, 6, 8	10

The lateral stress σ_2 and the axial stress σ_1 were added to the predetermined V value, then the lateral stress σ_2 was kept unchanged, and the axial stress continued to increase until the specimen was destroyed.

3. Analysis of compressive strength

3.1. The influence of lateral stress

When both the loading rate V and the dip angle β of the joint were fixed, the compressive strength σ_b increased with lateral stress σ_2 (Figure 3).

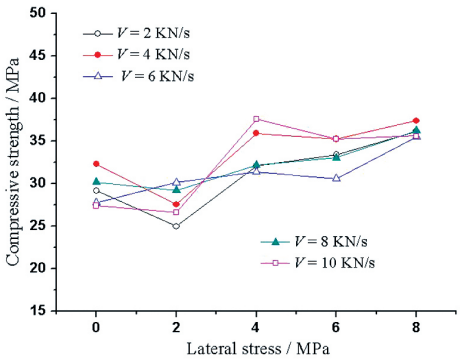

(a) $\beta = 0°$

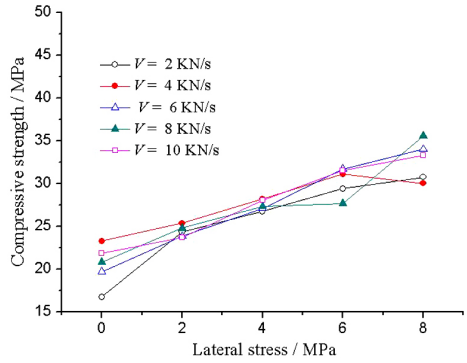

(b) $\beta = 30°$

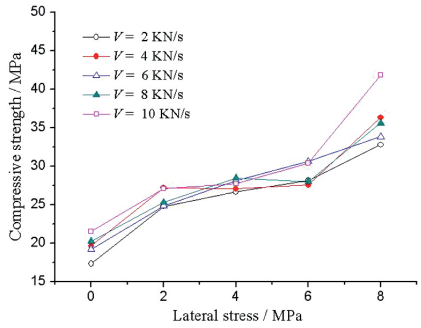

(c) β = 45°

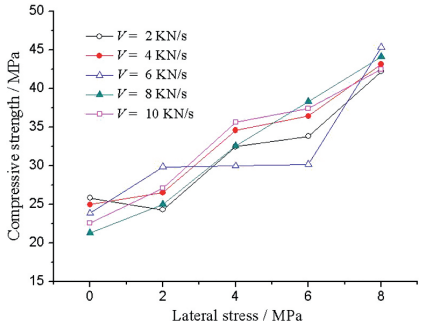

(d) β = 60°

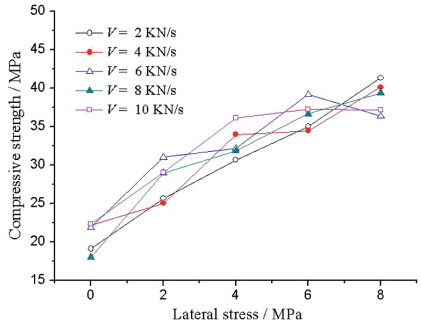

(e) β = 90°

Fig. 3. The variation law of the test value of biaxial compressive strength with the lateral stress (the loading rate was fixed)

3.2. The influence of the loading rate

When both the lateral stress σ_2 and dip angle β of the joint were fixed, the evolution law of compressive strength σ_b with the loading rate $V$was not obvious (Figure 4).

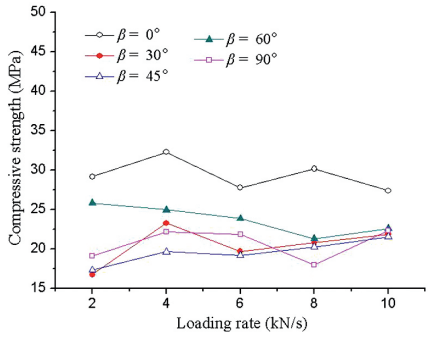

(a) lateral stress is 0 MPa

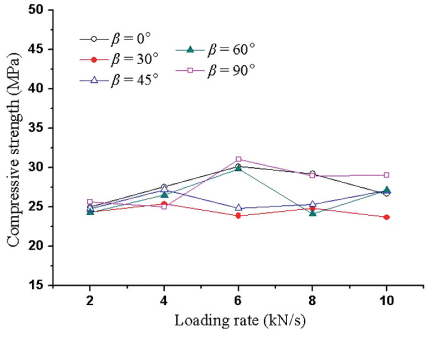

(b) lateral stress is 2 MPa

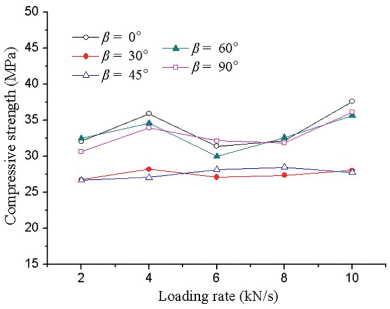

(c) lateral stress is 4 MPa

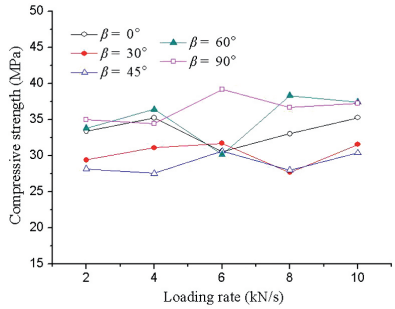

(d) lateral stress is 6 MPa

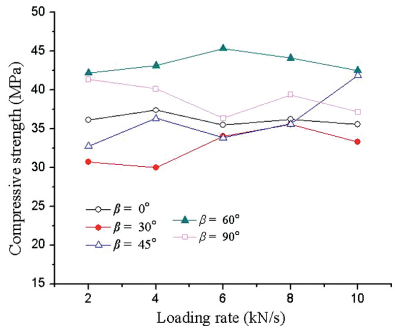

(e) lateral stress is 8 MPa

Fig. 4. The variation law of the test value of biaxial compressive strength with the loading rate (the lateral stress was fixed)

3.3. The influence of the dip angle of the joint

When both the lateral stress σ_2 and loading rate V were fixed, the compressive strength σ_b first decreased, then increased and decreased again with the increase of the dip angle β (Figure 5). When the dip angle β was 30° or 45°, the compressive strength reached the minimum value.

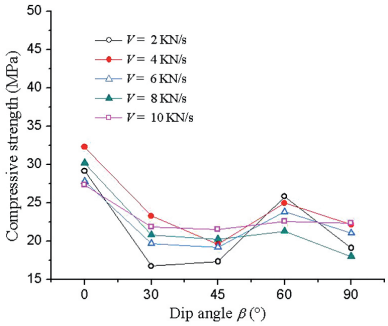

(a) lateral stress is 0 MPa

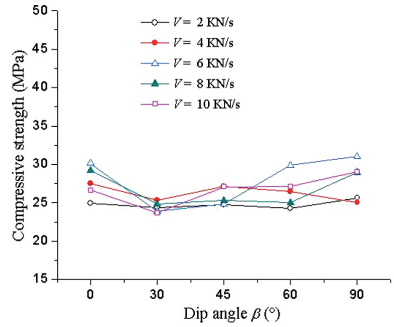

(b) lateral stress is 2 MPa

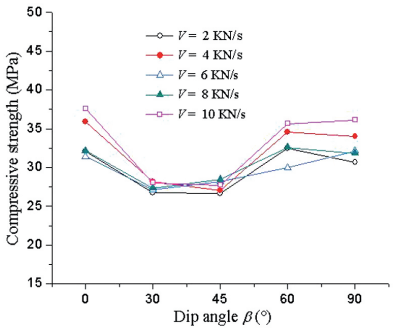

(c) lateral stress is 4 MPa

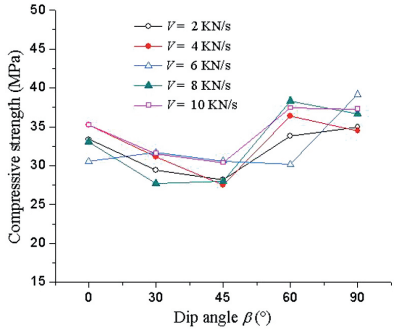

(d) lateral stress is 6 MPa

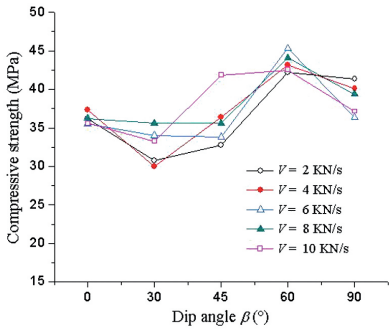

(e) lateral stress is 8 MPa

Fig. 5. The variation law of the test value of biaxial compressive strength with the dip angle of the joint (the lateral stress was fixed)

4. Numerical calculation results

4.1. The numerical model

In this study, PFC^{2D} was used for numerical simulations. The specimen's height and width were 100 and 100 mm, respectively. It was mainly through numerical simulation of the uniaxial compression test. When the numerical simulation results of uniaxial compression were close to the test results, the group of parameters was used for further numerical simulations. The parameters are listed in Table 2.

Table 2. PFC calculation parameters

Maximum particle size R_{max} (mm)	Particle diameter ratio R_{max}/R_{min}	Grain density (kg/m^3)	Friction factor μ	Particle stiffness ratio k_n/k_s	Multiplier ratio of parallel bond radius λ
0.4	2.2	2700	0.5	1.0	1.0

The parallel bond modulus was 1.0 GPa, the average normal bond strength was 9.0 MPa, the average tangential bond strength was 9.0 MPa, and the effective modulus was 0.8 GPa.

4.2. The influence of lateral stress

When both the loading rate V and the dip angle β of the joint were constant, the compressive strength σ_b increased with the lateral stress σ_2. The experimental law was identical to the numerical law (Figure 6).

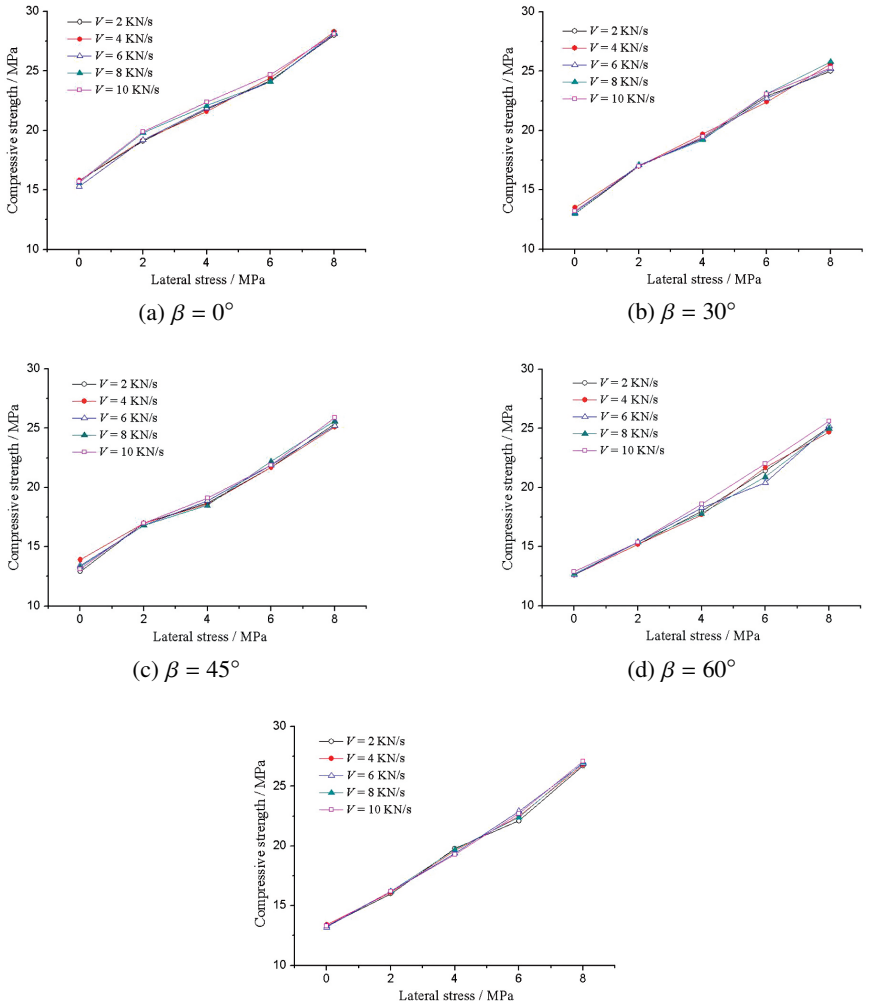

(a) $\beta = 0°$ (b) $\beta = 30°$

(c) $\beta = 45°$ (d) $\beta = 60°$

(e) $\beta = 90°$

Fig. 6. The variation law of the numerical value of biaxial compressive strength with the lateral stress (the loading rate was fixed)

4.3. The influence of loading rate

When both the lateral stress σ_2 and dip angle β of the joint were fixed, the compressive strength did not significantly change with the increase of the loading rate V (Fig. 7). Therefore, the loading rate V had no significant effect on the biaxial compressive strength σ_b.

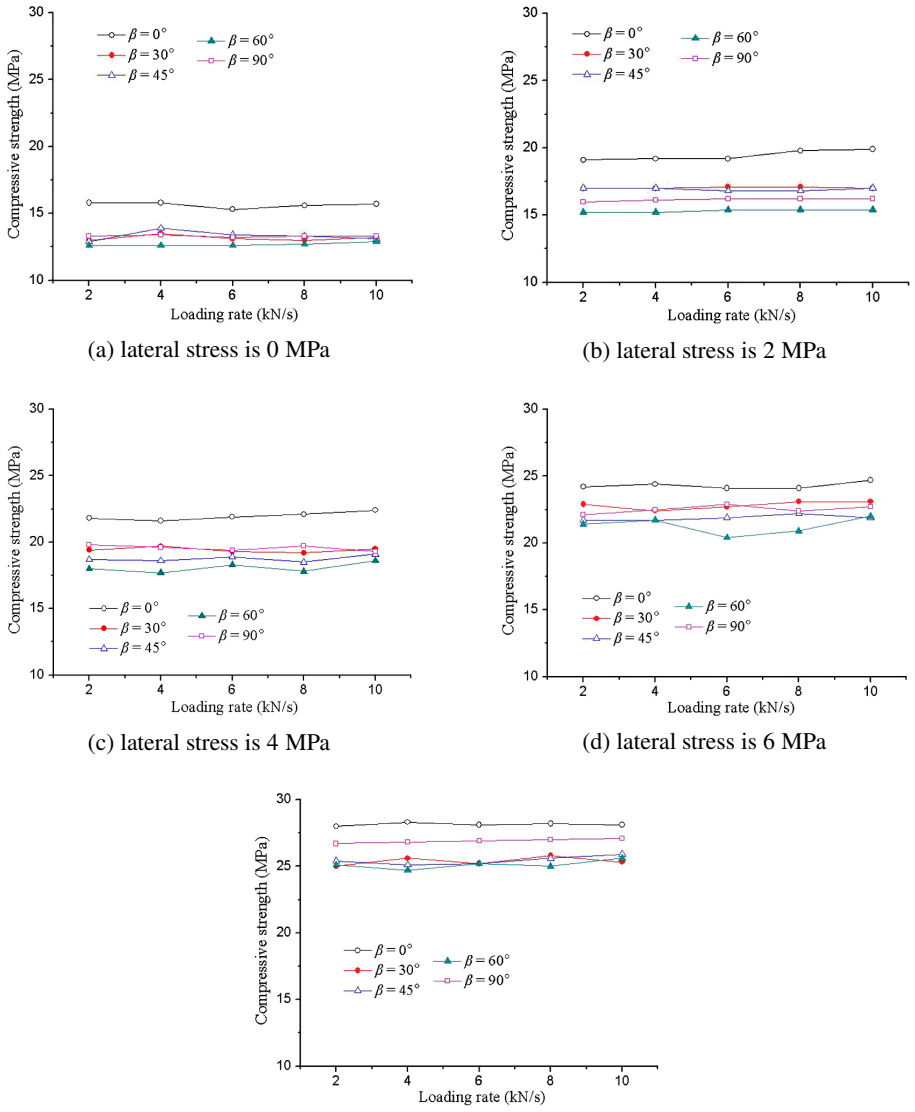

(a) lateral stress is 0 MPa

(b) lateral stress is 2 MPa

(c) lateral stress is 4 MPa

(d) lateral stress is 6 MPa

(e) lateral stress is 8 MPa

Fig. 7. The variation law of the numerical value of biaxial compressive strength with the loading rate (the lateral stress was fixed)

4.4. The influence of the dip angle of the joint

When both the lateral stress σ_2 and loading rate V were fixed, the compressive strength σ_b first decreased and then increased with increasing the dip angle β of the joint (Figure 8). When the dip angle β of the joint was 0°, the compressive strength of the specimen reached the maximum; when the dip angle β of the joint was 60°, the compressive strength of the sample reached the minimum.

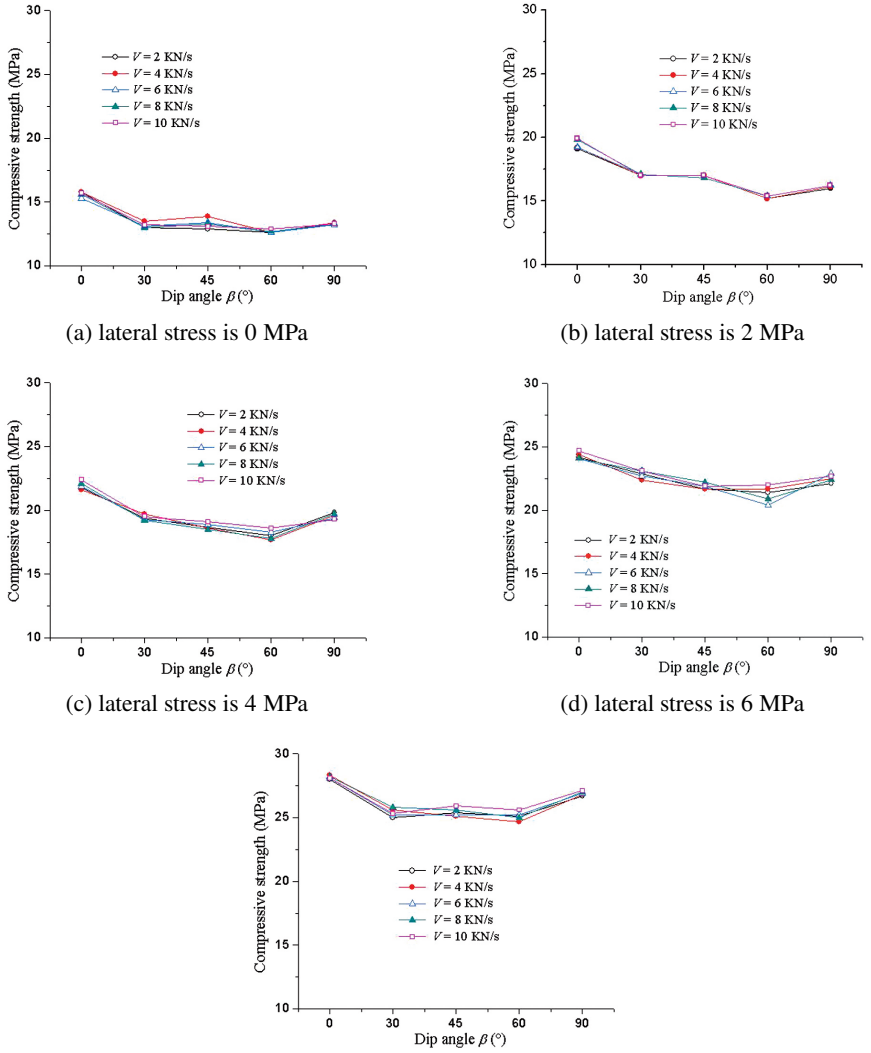

(a) lateral stress is 0 MPa

(b) lateral stress is 2 MPa

(c) lateral stress is 4 MPa

(d) lateral stress is 6 MPa

(e) lateral stress is 8 MPa

Fig. 8. The variation law of the numerical value of biaxial compressive strength with a dip angle of the joint (the lateral stress was fixed)

5. Analysis of the evolution law of crack

5.1. The influence of lateral stress

For the case where the dip angle β of the joint was 30° and the loading rate V was 4 kN/s, the influence of lateral stress on the rupture of the specimen was obtained from experiments and numerical simulations, as shown in Figures 9 and 10. Circled numbers 1–3 indicate the preset joint, the wing cracks developed on the side of the preset joint, and secondary cracks generated at the tips of the preset joint, respectively.

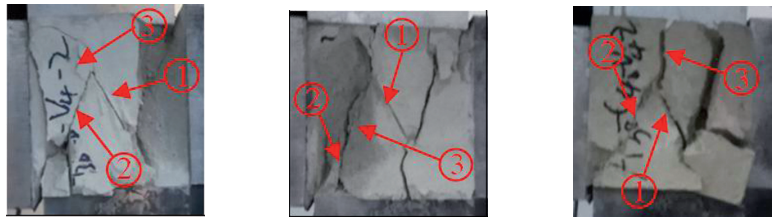

(a) lateral stress is 0 MPa

(b) lateral stress is 2 MPa

(c) llateral stress is 4 MPa

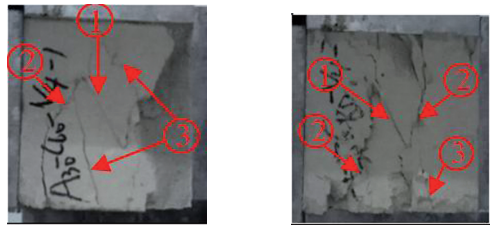

(d) lateral stress is 6 MPa

(e) lateral stress is 8 MPa

Fig. 9. The influence of lateral stress on the rupture of the specimen obtained from experiments

The crack law of the specimen obtained from the test revealed that: (1) the preset joint was closed and a wing crack was generated at both ends of the preset joint, and the wing crack gradually developed toward the diagonal of the specimen (the left wing crack developed to the lower left corner of the specimen, and the right-wing crack developed to the upper right corner of the specimen); (2) secondary cracks occurred at both ends of the preset crack or on the preset crack; (3) the crack connection caused the free surface layer to peel off, and the specimen was destroyed eventually. The size of the lateral stress affected the location and propagation of the secondary cracks, but the effect on the generation of wing cracks and the final failure mode of the specimen was not obvious.

The crack law of the specimen obtained by numerical simulations showed that: (1) when there was no lateral stress, a wing crack was generated at both ends of the prefabricated crack, and the wing crack developed in the loading direction of the lateral stress; (2) when

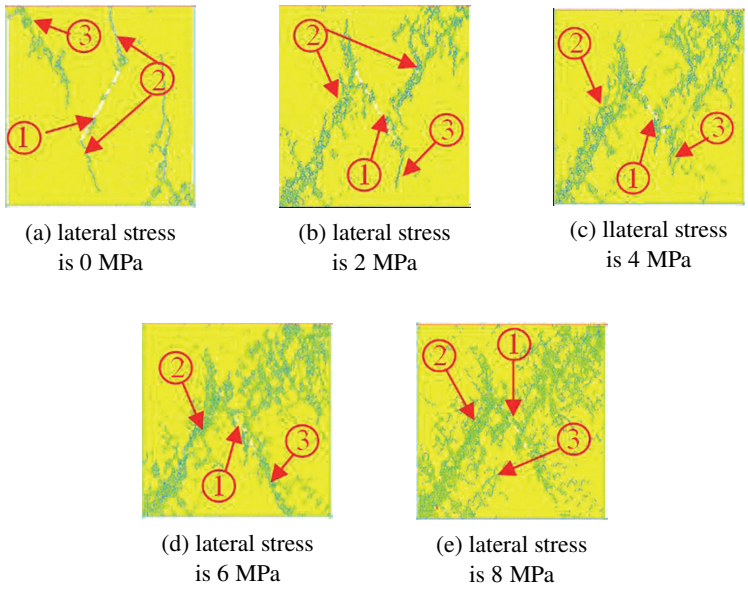

(a) lateral stress is 0 MPa

(b) lateral stress is 2 MPa

(c) llateral stress is 4 MPa

(d) lateral stress is 6 MPa

(e) lateral stress is 8 MPa

Fig. 10. The influence of lateral stress on the rupture of the specimen obtained from numerical simulations

there was lateral stress, wing cracks and secondary cracks occurred at both ends of the preset joint, which developed toward the corners of the specimen or the loading direction of the lateral stress. Finally, these cracks connected with the sides or corners of the specimen, forming a through crack and causing the free surface layer to peel off, destroying the specimen.

Both tests and numerical simulations showed that the development of wing cracks and secondary cracks made the cracks penetrate, ultimately leading to the specimens' destruction, and the wing cracks played a leading role in the specimens' destruction. The sample mainly presented a tensile failure.

5.2. The influence of the loading rate

The effect of loading rate V on the crack law of the specimen was investigated through experiments and numerical simulations when the dip angle of the joint was 30° and the lateral stress σ_2 was 2 MPa, as shown in Table 3.

With the increase of the loading rate V, the location of the secondary cracks changed slightly; however, the generation, propagation, and evolution laws of wing cracks did not change, and the final failure mode of the specimen did not change significantly. The sample mainly showed a tensile failure; therefore, the effect of the loading rate V on the crack evolution law of the specimen was not obvious.

Table 3. The influence of the loading rate on the fracture diagram of a specimen

Loading rate V (KN/s)	Fracture process obtained by experiment				Final destruction diagram obtained by numerical simulation
	When uncompressed	The preset joint was closed, and wing cracks and secondary cracks were generated	Crack connection	Destruction	
2		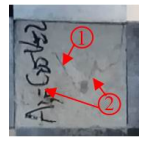			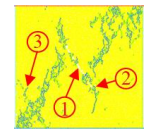
4					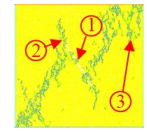
6					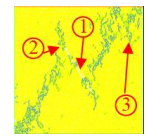
8					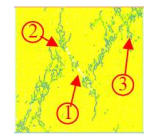
10			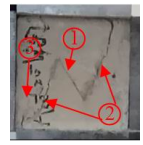	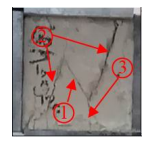	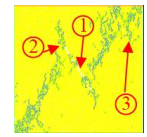

5.3. The influence of the dip angle of the joint

The effect of the dip angle of the joint on the crack law of the specimen was investigated through experiments and numerical simulations when the loading rate was 4 kN/s and the lateral stress was 2 MPa, as shown in Table 4.

When the dip angle of the joint was 0°, the preset joint did not close during the biaxial compression process, and wing cracks were generated at both ends of the preset joint. The wing cracks developed up and down, and finally connected the boundaries of the specimen,

Table 4. The influence of the dip angle of the joint on the fracture diagram of the specimen

Dip angle β (°)	Fracture process obtained by experiment				Final destruction diagram obtained by numerical simulation
	When uncompressed	The preset joint was closed, and wing cracks and secondary cracks were generated	Crack connection	Destruction	
0					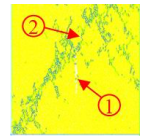
30		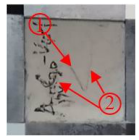		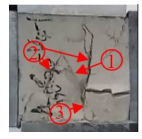	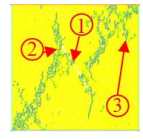
45					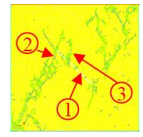
60		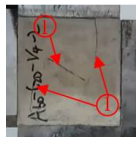	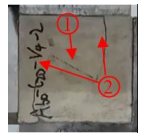	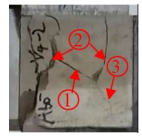	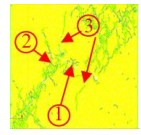
90	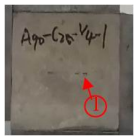				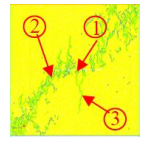

and the specimen was damaged; When the dip angle of the joint was 30, 45, and 60°, obvious wing cracks and secondary cracks were generated at both ends of the preset joint, and there were more secondary cracks; when the dip angle of the joint was 90°, wing cracks were also generated at both ends of the preset joint, and the number of secondary cracks was relatively smaller. The sample mainly presented a tensile failure.

6. Conclusions

In this paper, the biaxial dynamic compression test and PFC^{2D} numerical simulations of cement mortar specimens with a single preset joint were carried out to study the influence of lateral stress σ_2, loading rate V, and the dip angle β of the joint on the biaxial compressive strength of specimens and the crack evolution law.

1. When both the loading rate V and the dip angle β of the joint were fixed, the compressive strength σ_b gradually increased with the lateral stress σ_2 increase. The lateral stress magnitude affected the location and expansion of the secondary cracks, but it had no obvious effect on the occurrence of wing cracks and the final failure mode of the specimen.
2. When the lateral stress σ_2 and the dip angle β of the joint were fixed, the change of the compressive strength σ_b with the loading rate V was not obvious. The change of the loading rate V had a slight effect on the location of secondary cracks, and had no obvious effect on the generation of wing cracks and the final failure mode.
3. When both the lateral stress σ_2 and the loading rate V were fixed, the compressive strength σ_b first decreased, then increased and decreased again with the dip angle (of joint) increase. The number of secondary cracks in the specimen also showed obvious changes.
4. Both tests and numerical simulations showed that the development of wing and secondary cracks resulted in penetrating cracks, ultimately leading to the specimens' destruction. The wing cracks played a leading role in the destruction process of the specimens. The sample mainly presented a tensile failure.

Acknowledgements

This work was supported by the Open Research Fund of Hunan Provincial Key Laboratory of Hydropower Development Key Technology (Grant No. PKLHD202002), the Open Research Fund of State Key Laboratory of Geohazard Prevention and Geoenvironment Protection (Grant no. SKLGP2021K020) and the Open Research Fund of Engineering Research Center of Underground Mine Construction, Ministry of Education (Grant No. JYBGCZX2020101).

References

[1] P.H.S.W. Kulatilake, B. Malama, and J. Wang, "Physical and particle flow modeling of jointed rock block behavior under uniaxial loading", *International Journal of Rock Mechanics and Mining Sciences*, vol. 38, no. 5, pp. 641-657, 2001, DOI: 10.1016/S1365-1609(01)00025-9.

[2] H. Lee and S. Jeon, "An experimental and numerical study of fracture coalescence in pre-cracked specimens under uniaxial compression", *International Journal of Solids and Structures*, vol. 48, no. 6, pp. 979–999, 2011, DOI: 10.1016/j.ijsolstr.2010.12.001.

[3] X. Chen, Z. H. Liao, and X. Peng, "Cracking process of rock mass models under uniaxial compression", *Journal of Central South University*, vol. 20, pp. 1661–1678, 2013, DOI: 10.1007/s11771-013-1660-2.

[4] R.H. Cao, P. Cao, X. Fan, et al., "An experimental and numerical study on mechanical behavior of ubiquitous-joint brittle rock-like specimens under uniaxial compression", *Rock Mechanics and Rock Engineering,* vol. 49, pp. 4319–4338, 2016, DOI: 10.1007/s00603-016-1029-6.

[5] S.Q. Yang, W.L. Tian, Y.H. Huang, et al., "An experimental and numerical study on cracking behavior of brittle sandstone containing two non-coplanar fissures under uniaxial compression", *Rock Mechanics and Rock Engineering*, vol. 49, pp. 1497–1515, 2016, DOI: 10.1007/s00603-015-0838-3.

[6] Y.L. Zhao, L.Y. Zhang, W.J. Wang, et al., "Cracking and stress-strain behavior of rock-like material containing two flaws under uniaxial compression", *Rock Mechanics and Rock Engineering*, vol. 49, pp. 2665–2687, 2016, DOI: 10.1007/s00603-016-0932-1.

[7] B. Zhang, S.C. Li, K.W. Xia, et al., "Reinforcement of rock mass with cross-flaws using rock bolt", *Tunnelling and Underground Space Technology*, vol. 51, pp. 346–353, 2016, DOI: 10.1016/j.tust.2015.10.007.

[8] C.C. Huang, W.D. Yang, K. Duan, et al., "Mechanical behaviors of the brittle rock-like specimens with multi-nonpersistent joints under uniaxial compression", *Construction and Building Materials*, vol. 220, pp. 426–443, 2019, DOI: 10.1016/j.conbuildmat.2019.05.159.

[9] S.Q. Yang, Y.H. Huang, and P.G. Ranjith, "Failure mechanical and acoustic behavior of brine saturated sandstone containing two pre-existing flaws under different confining pressures", *Engineering Fracture Mechanics*, vol. 193, pp. 108–121, 2018, DOI: 10.1016/j.engfracmech.2018.02.021.

[10] Z.P. Xiang, H.L. Wang, W.Y. Xu, and L. Li, "Mechanical behavior of rock-like specimens with hidden smooth joints under triaxial compression", *Journal of Materials in Civil Engineering*, vol. 31, no. 7, 2019, DOI: 10.1061/(ASCE)MT.1943-5533.0002787.

[11] W. Yao, Y.Y. Cai, J. Yu, et al., "Experimental and numerical study on mechanical and cracking behaviors of flawed granite under triaxial compression", *Measurement*, vol. 145, pp. 573–582, 2019, DOI: 10.1016/j.measurement.2019.03.035.

[12] M. Prudencio and M. Van Sint Jan, "Strength and failure modes of rock mass models with non-persistent joints", *International Journal of Rock Mechanics & Mining Sciences*, vol. 44, no. 6, pp. 890–902, 2007, DOI: 10.1016/j.ijrmms.2007.01.005.

[13] X. Fan, P.H.S.W. Kulatilake, X. Chen, et al., "Crack initiation stress and strain of jointed rock containing multi-cracks under uniaxial compressive loading: A particle flow code approach", *Journal of Central South University*, vol. 22, pp. 638–645, 2015, DOI: 10.1007/s11771-015-2565-z.

[14] S.Q. Yang, Y.H. Huang, P.G. Ranjith, et al., "Discrete element modeling on the crack evolution behavior of brittle sandstone containing three fissures under uniaxial compression", *Acta Mechanica Sinica,* vol. 31, no. 6, pp. 871–889, 2015, DOI: 10.1007/s10409-015-0444-3.

[15] R.H. Cao, P. Cao, H. Lin, et al., "Mechanical behavior of brittle rock-like specimens with pre-existing fissures under uniaxial loading experimental studies and particle mechanics approach", *Rock Mechanics and Rock Engineering*, vol. 49, pp. 763–783, 2016, DOI: 10.1007/s00603-015-0779-x.

[16] X.X. Yang, P.H.S.W. Kulatilake, X. Chen, et al., "Particle Flow Modeling of Rock Blocks with Nonpersistent Open Joints under Uniaxial Compression", *International Journal of Geomechanics*, vol. 16, no. 6, pp. 1–17, 2016, DOI: 10.1061/(ASCE)GM.1943-5622.0000649.

Received: 2022-06-25, Revised: 2022-11-09